

# An Origin for Harrisitic and Granular Olivine in the Rum Layered Suite, NW Scotland: a Crystal Size Distribution Study

**BRIAN O'DRISCOLL<sup>1</sup>\*, COLIN H. DONALDSON<sup>2</sup>, VALENTIN R. TROLL<sup>1</sup>, DOUGAL A. JERRAM<sup>3</sup> AND C. HENRY EMELEUS<sup>3</sup>**

<sup>1</sup>DEPARTMENT OF GEOLOGY, MUSEUM BUILDING, TRINITY COLLEGE DUBLIN, DUBLIN 2, IRELAND

<sup>2</sup>SCHOOL OF GEOGRAPHY AND GEOSCIENCES, UNIVERSITY OF ST. ANDREWS, ST. ANDREWS KY16 9AL, UK

<sup>3</sup>DEPARTMENT OF EARTH SCIENCES, UNIVERSITY OF DURHAM, SCIENCE LABORATORIES, SOUTH ROAD, DURHAM DH1 3LE, UK

**RECEIVED MARCH 6, 2006; ACCEPTED SEPTEMBER 19, 2006;  
ADVANCE ACCESS PUBLICATION NOVEMBER 7, 2006**

*Dendritic crystal morphologies occur in a number of igneous rocks and are thought to originate from the rapid growth of crystals, yet many examples of dendritic morphologies are found in plutonic igneous rocks where cooling rates should be low. Results from crystal size distribution (CSD) measurements on harrisitic olivines from Rum, Scotland, combined with estimated olivine growth rates, suggest that the characteristic skeletal hopper and branching olivines of harrisitic cumulates that are up to centimetres long, may have exceptionally short crystal growth times (several hours to several hundreds of days). This, together with very low calculated nucleation densities for harrisitic olivine, supports the interpretation of harrisite being a disequilibrium texture, developed in response to supersaturation of the magma in olivine. We propose that this supersaturation arose through undercooling of thin picrite sheets emplaced along the Rum magma chamber floor, beneath cooler resident magma. It is envisaged that the picrite sheets were largely free of suspended olivine crystals. Coupled with the olivine-enriched composition of the melt and the increasing cooling rate, this allowed homogeneous nucleation of olivine to set in at deeper undercooling and greater olivine supersaturation than if there had been plentiful suspended olivines to act as heterogeneous nuclei. The enhanced supersaturation caused rapid growth of olivine once nucleation began, with skeletal and dendritic shapes. It is suggested that the observed, interlayered sequences of harrisite and cumulus peridotite found throughout the Rum Layered Suite are a result of multiple episodes of harrisite crystallization resulting from picrite emplacement that alternated with periods of*

*crystal growth and accumulation in the main body of magma at lesser degrees of undercooling.*

KEY WORDS: *crystal size distribution; harrisite; crystal growth rates; Rum Layered Suite*

## INTRODUCTION

Harrisite is a term applied to a facies of coarse-grained basic or ultrabasic rock in the Rum Palaeocene layered intrusion (Fig. 1), NW Scotland. Both gabbroic and feldspathic peridotite varieties are found. Harrisite comprises >25% olivine crystals that have a dendritic or skeletal habit (Fig. 2a and b; Harker, 1908; Wadsworth, 1961; Wager & Brown, 1968; Donaldson, 1975a, 1977). Elongated olivines may be oriented at high angles to layers, a fact that led Wager *et al.* (1960) to describe the rock as a 'crescumulate' in their categorization of cumulate rocks. Such an arrangement of crystals resembles that of comb layering (e.g. Taubeneck & Poldervaart, 1960; Lofgren & Donaldson, 1975). However, examples of harrisite in which the olivines are oriented parallel or even obliquely to the layering are also observed, as are stellate olivines, implying some downward growth (Donaldson, 1977). Harrisitic texture is remarkably similar to skeletal olivine crystal forms observed in ultramafic Archaean hypabyssal and volcanic 'spinifex' rocks found in greenstone belts. Donaldson (1974) discussed the link between harrisite and spinifex,

\*Corresponding author. Telephone: 00353-1896-2675. Fax: 00353-1671-1199. E-mail: brodrisc@tcd.ie

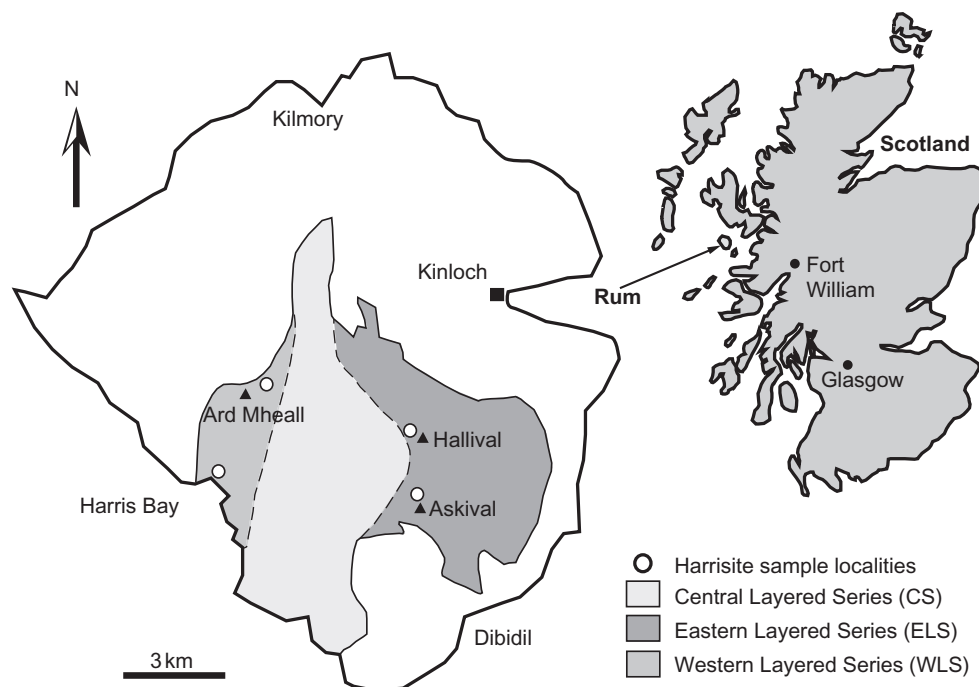


**Fig. 1.** Map of the Rum Layered Suite illustrating the localities of the Eastern, Western, and Central Layered Series. Harrisite sampling localities at Harris Bay, Ard Mheall, Hallival and Askival are also shown.

proposing a crystal morphological classification scheme that characterized the similarities between them.

Harrisite generally occurs interlayered with granular textured gabbro or feldspathic peridotite on Rum. Olivines in the latter rocks show a marked morphological and size contrast to harrisitic olivines. As well as being considerably smaller ( $< 2$  mm vs 2–1000 mm), olivine crystals in gabbro and feldspathic peridotite are typically sub-hedral in shape and are generally interpreted as cumulus in origin (Brown, 1956; Wadsworth, 1961; Emeleus *et al.*, 1996). Donaldson (1977) described a cyclic stratigraphy from gabbro or feldspathic peridotite up into harrisite in which small equant granular olivines are overlain by progressively larger and more deeply indented skeletal ‘hopper’ olivines (Figs 2c and 3). The main morphological changes within the harrisite are from subequant hopper and tabular hopper olivines to dendritic, branching crystal morphologies (Figs 2b and 3a). This change involves a 1500-fold decrease in the number of olivine crystals and grain-size increases of up to 1000 or more times (Donaldson, 1977). The upper contact of a harrisite layer with cumulate gabbro or peridotite is typically abrupt in both texture and grain size, an observation that led Wadsworth (1961) to suggest that it was recommencement of the settling of cumulus crystals that caused termination of harrisitic olivine formation.

Although it has been suggested that harrisitic olivine grew rapidly (Donaldson, 1974; Hort, 1998) and estimated growth rates (e.g. Henderson & Williams 1979;

$6.4 \times 10^{-5}$  mm/s) are four orders of magnitude greater than normal olivine crystal growth rates (e.g. Marsh, 1988;  $10^{-9}$  mm/s), no quantification of the actual crystal growth times has previously been presented for harrisite. In addition, no link has been proposed between the cyclic interlayering of harrisite and feldspathic peridotite and the inferred open-system behaviour (frequent replenishment by picrite magmas) of the Rum magma chamber. We combine published growth rates for harrisite and other examples of skeletal olivines with crystal size distribution (CSD) analyses, to estimate crystal growth times on the order of several hours to several hundred days for harrisitic olivine. A model is proposed in which very fast bursts of olivine growth accompanied repeated influxes of thin sheets of crystal-poor picrite magma at the base of the Rum magma chamber. This style of growth resulted from enhanced undercooling of the picrite and consequent enhanced olivine supersaturation of each sheet of new magma, before nucleation could set in. This model supports the view that the Rum magma chamber acted as an open or ‘leaky’ system (Brown, 1956; Tait, 1985; Emeleus *et al.*, 1996; Troll *et al.*, 2004).

### TEXTURAL QUANTIFICATION: CRYSTAL SIZE DISTRIBUTION (CSD) ANALYSIS

In recent years there has been a marked increase in the number of studies that look in detail at the quantification



**Fig. 2.** (a) Olivine 'dendrites' in harrisite, Harris Bay (1 Euro coin for scale at bottom right of image). (b) Intersecting skeletal olivine crystals in harrisite, Ard Mheall (crystal orientations highlighted; lens cap for scale in right centre of image). (c) Field photograph from Ard Mheall illustrating harrisite and granular textured peridotite layers (lens cap for scale in top left of image).

of crystal populations in rocks using advanced textural analysis techniques (Jerram & Kent, 2006). The key elements of the quantification of crystals in a rock are: (1) the size distribution (e.g. Marsh, 1998; Jerram, 2001); (2) the spatial distribution (e.g. Jerram *et al.*, 1996; Jerram & Cheadle, 2000); (3) the shape of crystals (e.g. Higgins, 1994; Mock & Jerram, 2005; Morgan & Jerram, 2006). In this study we employ the study of crystal size distributions in the quantification of harrisite and granular olivine textures. This requires the quantification of both the size and shape elements of the crystal population. Below we discuss CSD theory and its application to igneous systems, and then introduce the sampling methods and crystal growth rates used in the present study.

### CSD theory

CSD analyses are a quantitative measure of the number of crystals of a mineral per unit volume within a series of defined size intervals. Crystal size in igneous rocks carries information on growth rate and nucleation, and thus CSDs have been used as a method of determining some of the crystallization kinetics of magmatic systems independent of experimental approaches and thermodynamic or kinetic models (e.g. Cashman & Marsh, 1988; Resmini & Marsh, 1995; Marsh, 1998; Higgins, 2002a; Boorman *et al.*, 2004). A CSD plot is generally shown as a semi-logarithmic plot of population density (number of crystals per unit volume) against crystal size (maximum length).

Marsh (1988, 1998) suggested two end-member CSD models for igneous petrology; an open-system, or steady-state model and a closed-system (batch) model. Both of these models derive conservation equations for CSDs in different geological systems and show how these may be used to extract information on crystal growth rates and nucleation rates from population densities. The first open-system model describes a steady-state population balance of crystals growing into and out of a specific size range ( $L$ ), while at the same time physically circulating into and out of a system (Marsh, 1988). Continuous crystallization results in a straight, or log-linear, CSD plot. This model is described by the equation

$$n = n^{\circ} \exp(-L/G\tau)$$

where  $n$  is the population density,  $n^{\circ}$  is the nucleation density, the intercept of the curve on the  $y$ -axis,  $G$  is the crystal growth rate, and  $\tau$  is the magma chamber residence time or growth time of the crystals in the system. This steady-state model assumes that  $G$  is constant and independent of  $L$  and that nucleation rate is constant as well.

The second batch (Avrami-type) model of Marsh (1998) allows no input or output of crystals, and therefore cannot be described as a steady-state system. The volume of actively crystallizing magma decreases with time, conditions that might be satisfied by a lava lake

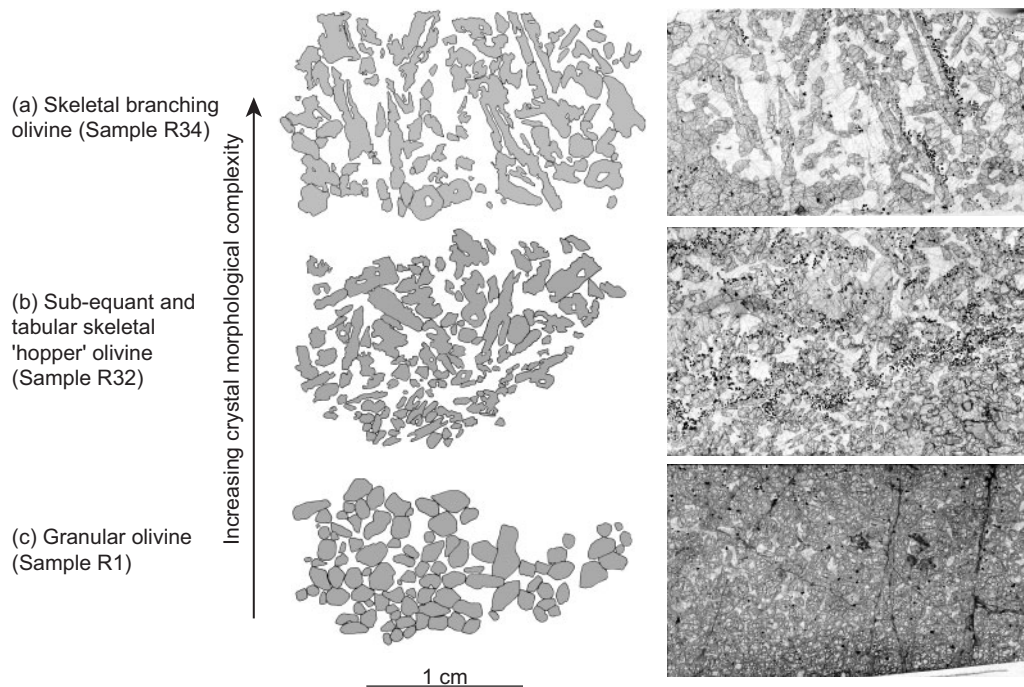


**Fig. 3.** Schematic cross-section through a sequence of layers (granular peridotite at base into overlying harrisitic feldspathic peridotite) at Ard Mheall using selected examples of original sample thin-section images together with corresponding 'edited', binary texture maps to illustrate the upwards increase in size and complexity of olivine crystal morphology. The 1 cm scale bar at the bottom of the image corresponds to both the photomicrographs and the digitized texture maps.

(e.g. Cashman & Marsh, 1988), but not a magma chamber (particularly an open-system magma reservoir). Marsh (1988, 1998) showed that under certain conditions (e.g. exponentially increasing nucleation rate with a constant growth rate), a batch system might also produce linear CSDs.

The texture produced in an open-system end-member model might be envisaged as resulting solely from the processes of nucleation and growth. The studies of Marsh (1988, 1998) suggest that the CSDs measured from such initial textures approximate a semi-logarithmic distribution, i.e. result in a log-linear plot. Such textures have been referred to as 'kinetic' in origin (e.g. Higgins, 2006). Kinking or curvature in the CSD plot profile has been attributed to processes such as crystal accumulation and removal (Marsh, 1998), compaction (Boorman *et al.*, 2004), mixing of crystal populations (Jerram *et al.*, 2003; Turner *et al.*, 2003) and post-nucleation crystal ageing caused by annealing or Ostwald ripening. Indeed, Higgins (2002a) and Boorman *et al.* (2004) have used CSD analysis to show that primary igneous textures may be strongly modified by both crystal coarsening and compaction-driven recrystallization.

Marsh (1998) examined a range of CSDs from a number of intrusive and extrusive igneous settings and found that

none of these systems showed CSDs typical of purely batch or open-system behaviour, each exhibiting instead a combination of the characteristics of each model. Although it is likely, therefore, that a given CSD reflects aspects of each end-member model, Marsh (1988, 1998) proposed generally applicable or effective values of crystal growth times for CSD interpretation based on the steady-state model

$$\ln(n) = -(1/G\tau)L + \ln(n^\circ)$$

or

$$m = -1/G\tau$$

where  $m$  is the slope of the CSD curve. Nucleation rate ( $\dot{f}$ ) may also be extracted from the CSD plot through the equation

$$\dot{f} = n^\circ G.$$

We will utilize the proposition of Marsh (1998) that initial (unmodified) 'kinetic' textures produce straight CSDs in our interpretation of the textural data presented here. We will also consider the observations by previous workers that the Rum magma chamber operated as an open system (e.g. Tait, 1985;

Renner & Palacz, 1987; Emeleus *et al.*, 1996; Troll *et al.*, 2004; Holness, 2005), to ensure that the CSDs are interpreted properly in the context of the magmatic system in question.

### Sampling methods

Harrisite occurs throughout the Rum layered intrusion but is most abundant in the western part of the Layered Suite at Ard Mheall and Harris Bay (Fig. 1), the latter being the type locality for the rock (Harker, 1908). The Layered Suite comprises the Eastern and Western Layered Series, considered to be lateral equivalents of one another, although at different structural levels (Emeleus *et al.*, 1996), subsequently intruded and separated by the younger Central Series (Fig. 1). Whereas the Eastern Layered Series is dominated by feldspathic peridotite and troctolite, the Central Series is mostly feldspathic peridotite, and the Western Layered Series is feldspathic peridotite in its upper reaches (Ard Mheall) and bytownite-bearing gabbro in its lower reaches (Harris Bay).

Sampling focused on the Western Layered Series, where a vertical traverse of 10 samples was collected through the sequence of feldspathic peridotite layers in the Ard Mheall area (Fig. 1). In addition, two samples were collected from Harris Bay and seven from the Eastern Layered Series; of the latter, four are from Units 10–13 on Askival and three are from Units 13–15 on Hallival (Fig. 1). A variety of olivine crystal morphologies were sampled, including granular grains from feldspathic peridotite to skeletal hopper and simple branching grains in harrisite. Sample numbers are given together with characteristic crystal morphologies in Table 1. It should be noted that very large, complex harrisitic olivines (larger than several centimetres in size) were not studied for reasons discussed in the next section.

### CSD analysis procedure

CSDs of harrisitic and granular olivines were measured in the following way. Individual crystals were identified and outlined on hard-copy overlays of high-resolution photomicrographs of single thin sections with the aid of a microscope. This texture overlay was then edited into a simple bitmap format before being opened into UTHSCSA ImageTool, an image analysis software package (Fig. 3). The image scale was set and the crystals were analysed for their area and the orientation and length of their long and short axes. The smallest crystals measured in this study were approximately 0.1 mm in size. These were the smallest grains observed at 25 times magnification and were easily large enough to be counted in the analysis. As all of the samples measured are holocrystalline, it is considered that all crystals have been measured for each sample, and we therefore take the

smallest grain size reported for each sample as the limit for that sample.

Initial CSD analysis was subsequently carried out as outlined by Higgins (2002a); the size distributions of the long axes of crystals were measured and corrected for 2D–3D effects using the method and software of Higgins (2000, CSDCorrections version 1.37). The CSD program, which has been used in many recent quantitative textural studies (Coogan *et al.*, 2002; Jerram *et al.*, 2003; Boorman *et al.*, 2004; Mock & Jerram, 2005), requires input of several other crystal measurements for each sample analysed. These include aspect ratio, calculated following the method of Morgan & Jerram (2006), and crystal roundness, calculated after Higgins (1994, 2000). Table 1 is a complete list of all of the quantitative textural data input into CSDCorrections in this study.

The intricate morphologies of some of the more complex harrisitic olivine crystal groups are far removed from the ideal crystal habit groupings assumed by the CSDCorrections program. These include the 'parallel-linked', 'chain-like', and 'radiate' morphologies of Donaldson (1975a), amongst others. A cut through such skeletal crystals could give the false impression in a thin section of many more (smaller) crystals than in reality. To avoid this problem, only samples with comparatively simple skeletal olivine morphologies were selected for study. Samples HBI, HB2, R15, R34 and ARH6 contained simple branching skeletal olivine crystals, generally not greater than 1.5 cm in length. Thin-sections of these crystals were studied to ensure that groups of apparently distinct crystals were not in optical continuity, i.e. were not linked in three dimensions, and hence did not misrepresent the CSDs of the rock. An average of 430 crystals were studied per sample and none had less than 200 crystals measured, consistent with the findings of Mock & Jerram (2005) and Gualda (2006) for accurate determination of the true CSD. This required that 3–4 thin-sections be measured per sample for most of the samples. In such cases, the grain-size data were then integrated and analysed together. Many samples are isotropic, but some of the harrisite samples exhibit a well-defined layer-parallel planar foliation defined by the alignment of elongate olivine crystals. In such cases, this was taken into account by the CSDCorrections software (Higgins, 2000).

Boorman *et al.* (2004) advocated caution when utilizing the CSDCorrections software. In particular, they highlighted two features of the program that affect CSDs calculated using crystal length (as the crystal size parameter) for plutonic rocks in particular. One is that the software assumes crystals of a given mineral will have euhedral shapes with fixed aspect ratios, an assumption that, although accurate for crystals in many volcanic rocks, will certainly not hold true for the skeletal and dendritic olivine crystal morphologies in harrisite.

Table 1: Sample identification numbers and olivine crystal morphologies together with the textural data input into CSDCorrections (1.37)

Sample	Crystal morphology	Sample area (mm <sup>2</sup> )	Vol. phase prop. (%)	Roundness	Fabric	No. of crystals	$L_{\max}$ (mm)
R1	Granular (1:1-2:1-7)	648-92	62-8	0-7	0	280	3-71
R2	Skeletal hopper (1:1-25:1-9)	1218-67	73-8	0-7	0	200	10-75
ARH1	Skeletal hopper (1:1-4:2-8)	2952-08	51	0-6	0	450	10-67
ARH2	Skeletal hopper (1:1-5:1-9)	3104-98	55	0-6	0	630	10-22
ARH3	Skeletal hopper (1:1-3:2-4)	3214	65	0-6	0	767	12-93
ARH6	Skeletal branching (1:1-5:3-6)	2138-45	46	0-5	0	744	8-26
P1	Granular (1:1-4:2-8)	1812	37	0-6	0	738	5-17
HB1	Skeletal branching (1:2:10)	997-67	30	0-4	0	309	12-32
HB2	Skeletal branching (1:2-5:9)	2083	31	0-5	0	584	10-66
R15	Skeletal branching (1:2-5:5)	1357-52	50	0-5	0-6	623	14-52
R16	Skeletal hopper (1:1-25:1-8)	1126-58	64-4	0-7	0	587	10-07
R17	Skeletal hopper (1:1-4:1-7)	1105-52	53	0-5	0-1	328	9-22
R31A	Skeletal hopper (1:1-7:2-3)	641-48	58	0-6	0-4	415	7-32
R31B	Granular (1:1-25:1-8)	508-51	38-9	0-7	0	344	3-69
R32	Skeletal hopper (1:1-6:3-2)	744-58	47-5	0-5	0-2	331	8-44
R33	Skeletal hopper (1:1-25:2)	687-45	57-3	0-7	0	357	6-89
R34	Skeletal branching (1:1-2:1-9)	847-14	79-4	0-7	0	200	9-16
R36A	Granular (1:1-2:1-8)	220-49	79-4	0-7	0	281	2-71
R36B	Skeletal hopper (1:1-6:3-2)	290-05	70-8	0-6	0-7	218	5-78
R37	Granular (1:1-25:1-7)	351-63	75-3	0-6	0	200	5-04

Aspect ratios calculated after Morgan & Jerram (2006).

The second is that CSDs calculated for samples containing crystals with high aspect ratios will produce flatter curves than those for samples with more equant grains, even though both samples may have an identical volume phase proportion (Higgins, 2002*b*; Boorman *et al.*, 2004). Boorman *et al.* (2004) suggested an alternative means by which the CSDCorrections software may be used for plutonic rocks to avoid the above problem. Instead of taking major axis length as a grain-size parameter, Feret length, the length of a square with an area equal to the measured area of the grain, is used. This requires that aspect ratios for all crystals be 1:1:1 and that the roundness factor is zero. This approach gives a good correlation between measured volume phase proportions and those calculated by CSDCorrections. However, as stated by Boorman *et al.* (2004), ‘uncertain error is introduced in the cut section and fabric correction by the assumption of cubic shape’, causing CSD curves to have much steeper slopes. This is well illustrated in Fig. 4, which shows two CSDs for sample R15 of this study, one calculated using Feret length, the other using maximum crystal length. In addition, Mock & Jerram (2005) and Morgan

& Jerram (2006) showed that assumption of a spherical crystal shape (with a similar aspect ratio to a cube) gives a poor estimation of CSD slope. As calculation of crystal growth times is dependent on the slope of the CSD, we do not employ the Feret length method in this study. To overcome issues raised by Boorman *et al.* (2004), we use the updated version of the CSDCorrections software (version 1.37; Higgins, 2000), which allows the correction of the CSD to the measured volume phase proportion—equivalent to a chemical analysis normalized to 100%. We also use the extensive CSDslice crystal shape database of Morgan & Jerram (2006) to obtain better objective estimates of olivine crystal habits in the Rum samples. Figure 5 is a plot of I/L vs S/I, where S, I and L are the short, intermediate and long axes of the crystal aspect ratios, respectively (as calculated by CSDslice), and highlights the morphological differences in olivine crystal shapes.

Closure limits have also been calculated for the CSD data following the methods outlined by Higgins (2002*b*). In principle, closure limits do not allow the calculated crystal content of a rock to exceed 100%, although where

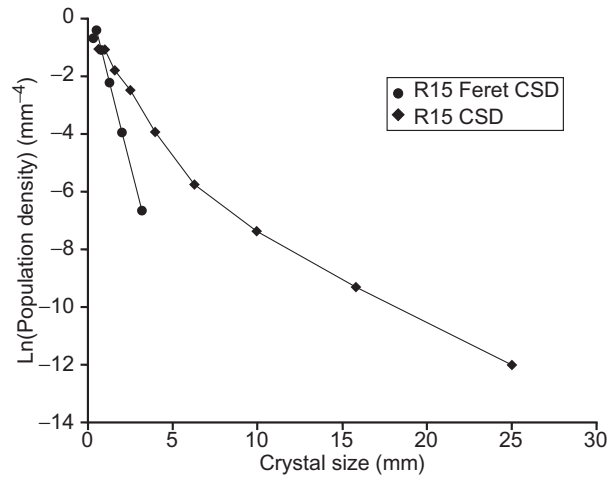


**Fig. 4.** Two plots of CSD data for sample R15, illustrating the contrasting slope magnitudes returned by the CSDCorrections (1.37) program for the different crystal size parameters: major axis length and Feret length.

chemical or thermal effects limit growth of a specific mineral phase, closure occurs at a lower volumetric phase proportion (Higgins, 2002*b*). Plots of characteristic length (see below for definition) vs intercept, characteristic length vs volume phase proportion (%), slope vs intercept and slope vs  $L_{\max}$  reflect CSD closure and can be used to further investigate and verify CSD data (e.g. Marsh, 1998; Higgins, 2002*b*; Boorman *et al.*, 2004). These additional plots will also be utilized in this study to fully constrain the CSD data and are discussed in the CSD results section along with the classic semi-log plots of population density (number of crystals per unit volume) against crystal size (maximum length). Calculation of characteristic lengths have been carried out using the equations of Higgins (2002*b*) as follows:

$$m = -1/C_i$$

and

$$V_i = 6\sigma n_{i0} C_i^4$$

where  $C_i$  is the characteristic length,  $V_i$  is the volumetric phase proportion,  $\sigma$  is a shape factor, and  $n_{i0}$  is the final nucleation density. The latter equation is for straight CSDs only, a requirement fulfilled by the CSD plots in this study. Volumetric phase proportions were obtained by measuring modal abundances of mineral phases directly from the digitized thin-section images.  $L_{\max}$  was calculated as the average of the four largest grains of the crystal population for each sample.

### Olivine growth rates

As described above, the slope of a CSD gives a measure of  $G\tau$ , and if a value for  $G$  is known, crystal growth time

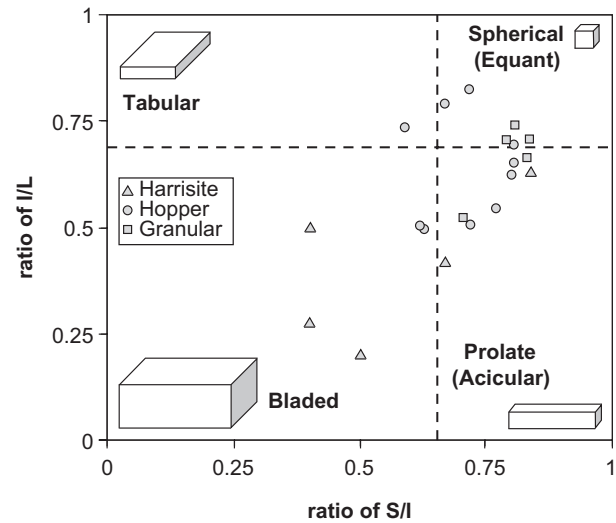


**Fig. 5.** Granular and harrisitic olivine crystal morphology plotted in terms of the variation in the three major crystal axes (as calculated by CSDslice; Morgan & Jerram, 2006). The positions of schematic tabular, cubic, acicular and bladed crystal shapes are also illustrated for comparison.

in the magma chamber can be estimated. Although typical crystal growth rates for minerals, both silicates and oxides, have been quoted as being between  $10^{-10}$  and  $10^{-9}$  mm/s (Marsh, 1988, 1996; Cashman, 1993; Higgins, 1996), studies carried out on crystals that have grown in a melt supersaturated with respect to their constituent elements show that these crystals may have grown considerably faster. In particular, a sizeable body of work has been carried out on anhedral (hopper, skeletal, and dendritic) olivine crystals (Donaldson, 1975*a*, 1975*b*, 1976, 1977; Jambon *et al.*, 1992; Roggensack, 2001; Faure *et al.*, 2003; Kohut & Nielsen, 2004; Zieg & Lofgren, 2006), which suggests that crystal growth rates in the range  $10^{-5}$ – $10^{-7}$  mm/s are more typical of these crystals.

An independent estimate of olivine growth rates in the Rum cumulates was obtained by Henderson & Williams (1979) from the distribution of uranium between crystals and magma. They measured the uranium contents of olivines of different shapes and found that the more skeletal the shape, the greater the U content (Table 2). Using the estimate of Henderson *et al.* (1971) of the magma's uranium content, Henderson & Williams (1979) employed the Burton *et al.* (1953) model of diffusion-controlled crystal growth to compute model growth rates for the Rum olivines (Table 2). These show that the branching olivines grew at least five times faster than the granular crystals in interlayered cumulate. [The calculations required insertion of a value for the uranium diffusion

Table 2: Model growth rates of olivines of different shapes from Henderson & Williams (1979)

Morphology	Mean U (ng/g)	Growth rate (mm/s)
Granular	5	$1.2 \times 10^{-5}$
Hopper	5.99	$4.8 \times 10^{-5}$
Harrisitic	8.34	$6.4 \times 10^{-5}$

coefficient in basaltic magma. In the absence of this information, they used a figure of  $10^{-8}$  cm<sup>2</sup>/s measured by Seitz (1974) for Th diffusion in a synthetic melt of diopside, albite and anorthite. This figure differs little from an estimate of the diffusion coefficient of uranium in basalt melt at 1300°C ( $10^{-7.7}$  cm<sup>2</sup>/s) obtained by using Hoffman's (1980) empirical relationship between diffusion coefficient and ionic radius of the diffusing species.]

Although cooling rate, and hence growth rate, may be arbitrarily imposed in experimental systems to create skeletal crystal and dendritic morphologies, we believe that it is likely that the complex Rum harrisite textures crystallized in response to a cooling regime not typical of plutonic environments. Given the experimental evidence outlined above for very fast growth rates of skeletal and dendritic crystal morphologies, we believe that the calculated growth rates of Henderson & Williams for harrisitic olivine are likely to be accurate. In particular, values of  $(2-6) \times 10^{-6}$  mm/s (Donaldson, 1975*b*),  $(1.25-34.9) \times 10^{-6}$  mm/s (Kohut & Nielsen, 2004) and  $(1-6000) \times 10^{-7}$  mm/s (Jambon *et al.*, 1992) compare favourably with Henderson & Williams' computed value of  $6.4 \times 10^{-5}$  mm/s. We estimate a range of crystal growth times from our CSD plots for olivines in harrisite and feldspathic peridotite on Rum using the growth rates described above. The growth rates of Henderson & Williams give the shortest crystal growth times, so these are compared with the slowest growth rate quoted above, that of Jambon *et al.* (1992;  $1 \times 10^{-7}$  mm/s) for skeletal crystal growth and the implications for harrisite formation are discussed.

In addition, although the model growth rates of Henderson & Williams (1979) are consistent with those produced in laboratory experiments on skeletal crystals (Donaldson, 1975*b*; Jambon *et al.*, 1992; Kohut & Nielsen, 2004), not all of the crystals studied here are as complex. As typical growth rates for olivine are approximately  $10^{-9}$  mm/s we believe that the growth rates suggested by Henderson & Williams (1979) for granular (cumulus) olivine in the Rum magma chamber (e.g. samples R1, Pl, R31B, R36A and R37) are likely to be too fast.

To calculate realistic crystal growth times for granular olivine in the Rum magma chamber, the estimated value of Marsh (1988;  $10^{-9}$  mm/s) is employed as a lower limit of growth rate for granular peridotite samples.

## RESULTS

### CSD plots

The CSD results for all the samples are given in Table 3 and CSD plots for each sample are contained in Fig. 6. Data for different olivine crystal morphologies and sizes are generally consistent over the different sampled sites. All the curves are approximately log-linear for the larger size fractions and several have a well-developed 'humped', convex-up profile at smaller size fractions. Regression analysis was carried out on these curves in Microsoft Excel for a best-fit line through the log-linear portion of the plot, to calculate slope and intercept data from each. Although a minority of samples have slightly kinked CSDs (HBI, R15, R16, R17, R31A, and ARH3), characterized by changes to shallower slopes at the larger size intervals, these are also well described by one best-fit line through the whole curve; none has an  $R^2$  value of less than 0.89. CSD slopes for feldspathic peridotite samples with simple non-skeletal granular or polyhedral olivine morphologies (R1, Pl, R31B, R36A and R37) display the most pronounced 'humped' profiles at small crystal size fractions and have consistently relatively steep slopes between  $-1.78$  and  $-1.15$ . Consistency ( $-0.54$  to  $-0.31$ ) is also observed in the shallower slopes of the most complex skeletal branching morphologies studied (R15, HBI, HB2, R34 and ARH6). However, samples that contain hopper crystal morphologies (R2, ARH1, ARH2, ARH3, R16, R17, R31A, R32, R33, and R36B) span a wider range of slope values ( $-0.89$  to  $-0.48$ ).

We have defined the lower size limit of our CSDs at 0.1 mm and interpret the data based on the observation that there are no crystals in these rocks smaller than this size. The CSDs for harrisitic olivines are typically straight on semi-logarithmic plots of population density vs crystal size, especially at the larger size fractions. We interpret these disequilibrium textures as 'kinetic' textures (i.e. formed through nucleation and growth alone without significant postcumulus ripening or coarsening), although such textures may not be common in plutonic igneous rocks (see discussion below). This interpretation may not extend completely to the samples containing granular olivine crystals, some of which exhibit a 'humped' profile as outlined above. This issue and its bearing on the values of CSD slope obtained (and consequently the crystal growth times calculated) is also discussed in more detail in the section on the CSD data below.

We have also assessed the quality of the CSD data using closure limits (after Higgins, 2002*a*, 2002*b*;

Table 3: CSD results including slope and intercept data calculated by CSDCorrections for each sample\*

Sample	Crystal morphology	Slope	$\ln(n^\circ)$	Crystal growth time			Nucleation rate		
				$\tau_1$ (h)	$\tau_2$ (days)	$\tau_3$ (years)	$J_1$ ( $\text{mm}^{-3}/\text{s}$ )	$J_2$ ( $\text{mm}^{-3}/\text{s}$ )	$J_3$ ( $\text{mm}^{-3}/\text{s}$ )
R1	Granular (1:1-2:1-7)	-1.6492	1.3055	14		19.2	$4.4 \times 10^{-5}$		$3.7 \times 10^{-9}$
R2	Skeletal hopper (1:1.25:1-9)	-0.5997	-2.314	9.7	193		$4.8 \times 10^{-6}$	$9.9 \times 10^{-9}$	
ARH1	Skeletal hopper (1:1.4:2-8)	-0.4815	-2.563	12	240.4		$3.7 \times 10^{-6}$	$7.7 \times 10^{-9}$	
ARH2	Skeletal hopper (1:1.5:1-9)	-0.7381	-2.078	7.8	156.8		$6 \times 10^{-6}$	$1.3 \times 10^{-8}$	
ARH3	Skeletal hopper (1:1.3:2-4)	-0.5035	-2.199	11.5	229.9		$5.3 \times 10^{-6}$	$1.1 \times 10^{-8}$	
ARH6	Skeletal branching (1:1.5:3-6)	-0.5351	-1.507	8.1	216.3		$1.4 \times 10^{-5}$	$2.2 \times 10^{-8}$	
P1	Granular (1:1.4:2-8)	-1.252	0.8897	18.5		25.3	$2.9 \times 10^{-5}$		$2.4 \times 10^{-9}$
HB1	Skeletal branching (1:2:10)	-0.3151	-2.032	13.8	367.3		$8.4 \times 10^{-6}$	$1.3 \times 10^{-8}$	
HB2	Skeletal branching (1:2.5:9)	-0.3137	-2.238	13.8	369		$6.8 \times 10^{-6}$	$1.1 \times 10^{-8}$	
R15	Skeletal branching (1:2.5:5)	-0.4616	-1.543	9.4	250.7		$1.4 \times 10^{-5}$	$2.1 \times 10^{-8}$	
R16	Skeletal hopper (1:1.25:1-8)	-0.8069	-0.918	7.2	143.4		$1.9 \times 10^{-5}$	$4 \times 10^{-8}$	
R17	Skeletal hopper (1:1.4:1-7)	-0.8127	-1.771	7.1	142.4		$8.2 \times 10^{-6}$	$1.7 \times 10^{-8}$	
R31A	Skeletal hopper (1:1.7:2-3)	-0.8394	-1.026	6.9	137.9		$1.7 \times 10^{-5}$	$3.6 \times 10^{-8}$	
R31B	Granular (1:1.25:1-8)	-1.6545	1.082	14		19.2	$3.5 \times 10^{-5}$		$3 \times 10^{-9}$
R32	Skeletal hopper (1:1.6:3-2)	-0.746	-0.694	7.8	155.2		$2.4 \times 10^{-5}$	$5 \times 10^{-8}$	
R33	Skeletal hopper (1:1.25:2)	-0.8908	-0.514	6.5	129.9		$2.9 \times 10^{-5}$	$6 \times 10^{-8}$	
R34	Skeletal branching (1:1.2:1-9)	-0.5848	-2.015	9.9	197.9		$8.5 \times 10^{-6}$	$1.3 \times 10^{-8}$	
R36A	Granular (1:1-2:1-8)	-1.7797	1.9141	13		17.8	$8.1 \times 10^{-5}$		$6.7 \times 10^{-9}$
R36B	Skeletal hopper (1:1.6:3-2)	-0.8445	0.2326	6.9	137.1		$6.1 \times 10^{-5}$	$1.3 \times 10^{-7}$	
R37	Granular (1:1.25:1-7)	-1.1529	0.0634	20.1		27.5	$1.3 \times 10^{-5}$		$1.1 \times 10^{-9}$

\*Crystal growth times and nucleation rates for different olivine growth rates are also included as follows:  $\tau_1$  and  $J_1$  are calculated using the values of growth rate proposed for Rum olivines by Henderson & Williams (1979);  $\tau_2$  and  $J_2$  for harrisitic and hopper olivines only, calculated using the growth rate of Jambon *et al.* (1992;  $1 \times 10^{-7}$  mm/s);  $\tau_3$  and  $J_3$  for granular olivines only, calculated using the growth rate of  $10^{-9}$  mm/s (Marsh, 1988; Cashman, 1993). (See also text for discussion.)

Boorman *et al.*, 2004). A plot of characteristic grain length against intercepts, together with empirically calculated closure limits for harrisitic, hopper, and granular olivine crystals illustrates that our data fall well within the permitted range (Fig. 7a). A plot of CSD characteristic grain length against volume phase proportion (see Higgins, 2002a) highlights three distinct zones for each of the three crystal morphological groups (Fig. 7b; see also Fig. 5). Plots of CSD slope vs  $L_{\text{max}}$  and CSD slope vs intercept have been used by Marsh (1998) to determine elements of open (steady-state) system nucleation and growth and closed (batch) system nucleation and growth. The plot of slope against  $L_{\text{max}}$  for the Rum data shows a strong positive trend (Fig. 8a), whereas the plot of slope vs intercept exhibits negative trends and group-clustering for each of the granular, hopper and harrisitic crystal morphological sub-groups (Fig. 8b). This suggests that the CSD data might be interpreted as reflecting nucleation and growth of a single population of crystals in each case (Marsh, 1998).

### Crystal growth times

Crystal growth times have been calculated for the crystal populations of each sample (Table 3), using the slope of each CSD curve and the crystal growth rates for harrisitic olivine computed by Henderson & Williams (1979; Table 2). The times are exceptionally short, ranging from 7 to 20 h ( $\tau_1$  in Table 3). In general, the shortest times are given by the more complex olivine crystal geometries such as the skeletal branching and hopper morphological groups, even though these are larger in size than the granular olivines. Granular crystal morphologies typically give longer crystal growth times. Maximum crystal growth times have also been calculated for skeletal olivine morphologies using the upper growth rate limit of Jambon *et al.* (1992) as quoted above ( $\tau_2$  in Table 3). Although it is likely that these values are overestimates, they are still very short, ranging between 137 and 369 days. A set of crystal growth times for granular olivines is also presented in Table 3 ( $\tau_3$ ), based on a growth rate of  $10^{-9}$  mm/s as quoted above (Marsh, 1988; Cashman, 1993).

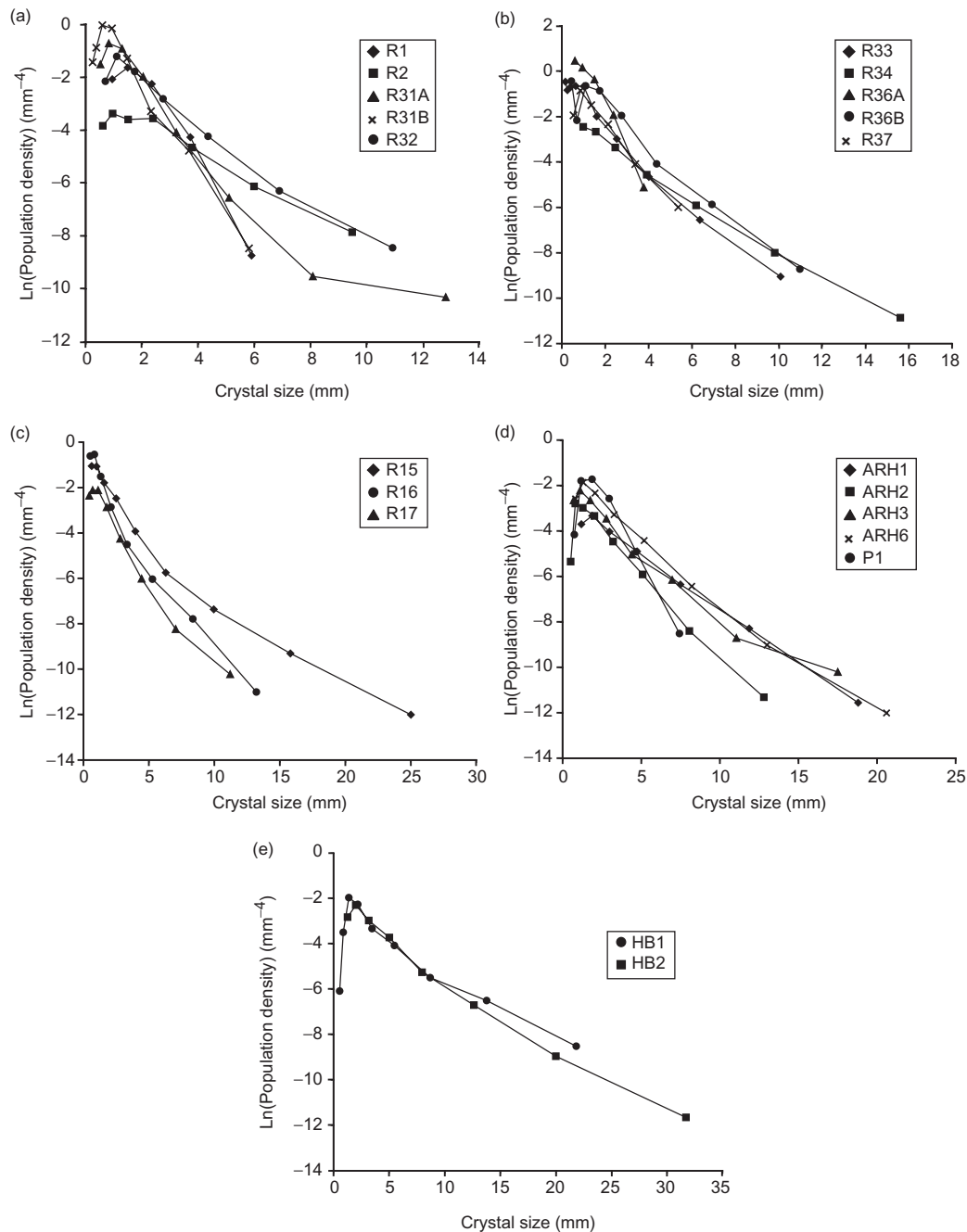


**Fig. 6.** CSD curves for samples from: (a) and (b) Ard Mheall; (c) Hallival; (d) Askival; (e) Harris Bay.

The calculated times are again short, ranging between 18 and 28 years, particularly when compared with values based on published growth rates (Marsh, 1988; Cashman, 1993; Higgins, 1996) that are three or four times higher (e.g. 50–80 years). (However, see below for the discussion of crystal growth times for granular olivine crystals.)

### Nucleation rates

Nucleation densities ( $n^\circ$ ) have been calculated from the  $y$ -axis intercepts on the CSDs, and are presented in Table 3. CSD intercepts ( $\ln [n^\circ]$ ) range from  $-2.6$  to  $1.9 \text{ mm}^{-4}$  ( $n^\circ = 7.4 \times 10^{-2}$  to  $6.7 \text{ mm}^{-4}$ ), values that are exceptionally low compared with nucleation densities [ $(2.07\text{--}4.55) \times 10^7 \text{ mm}^{-4}$ ] reported by Cashman & Marsh (1988)

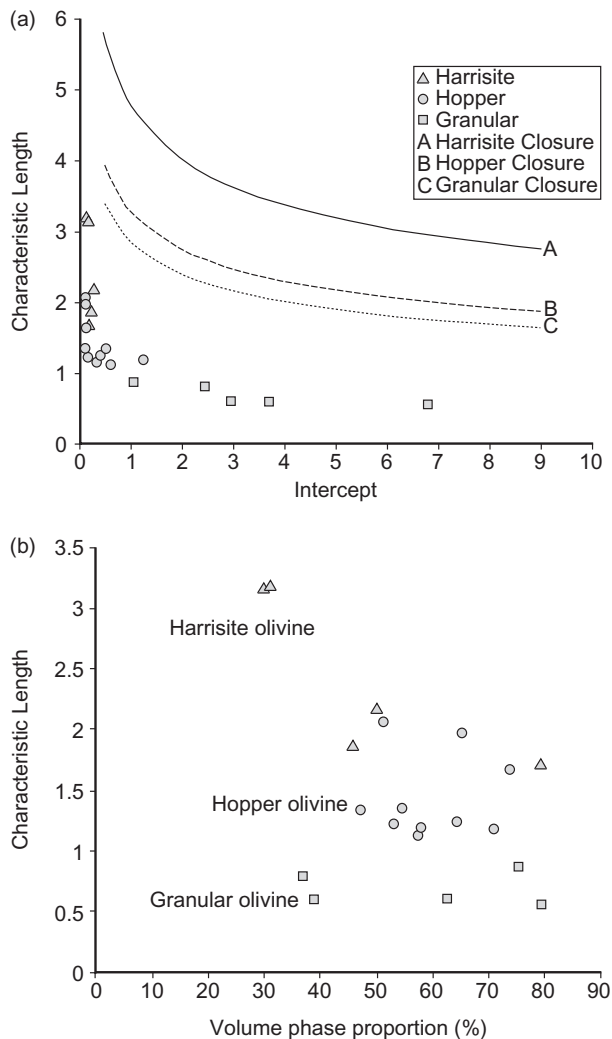


**Fig. 7.** (a) Plot of characteristic grain length vs intercept together with closure limits for all CSD data. (b) Plot of characteristic length vs volume phase proportion for harrisitic, hopper, and granular olivine crystal morphologies. Closure limits are calculated with approximate characteristic aspect ratios for each crystal morphology (after Morgan & Jerram, 2006).

for plagioclase from the Makaopuhi lava lake (Hawaii). Values of nucleation rate calculated using the growth rates of Henderson & Williams (1979) are in the range of  $(0.37\text{--}8.1) \times 10^{-5} \text{ mm}^{-3}/\text{s}$  ( $\bar{J}_1$  in Table 3). In general, the largest values of  $n^\circ$ , and consequently the largest values of  $\bar{J}$ , are given by feldspathic peridotite samples containing granular olivines (R1, P1, R31B, R36A and R37). Conversely, samples containing complex harrisitic morphologies (HB2, ARH1, ARH3, and R2) give the smallest values of  $n^\circ$  and much smaller values of  $\bar{J}$ , respectively.

However, the use of the growth rates above creates calculated nucleation rates ( $\bar{J}_1$ ) that are maxima for the

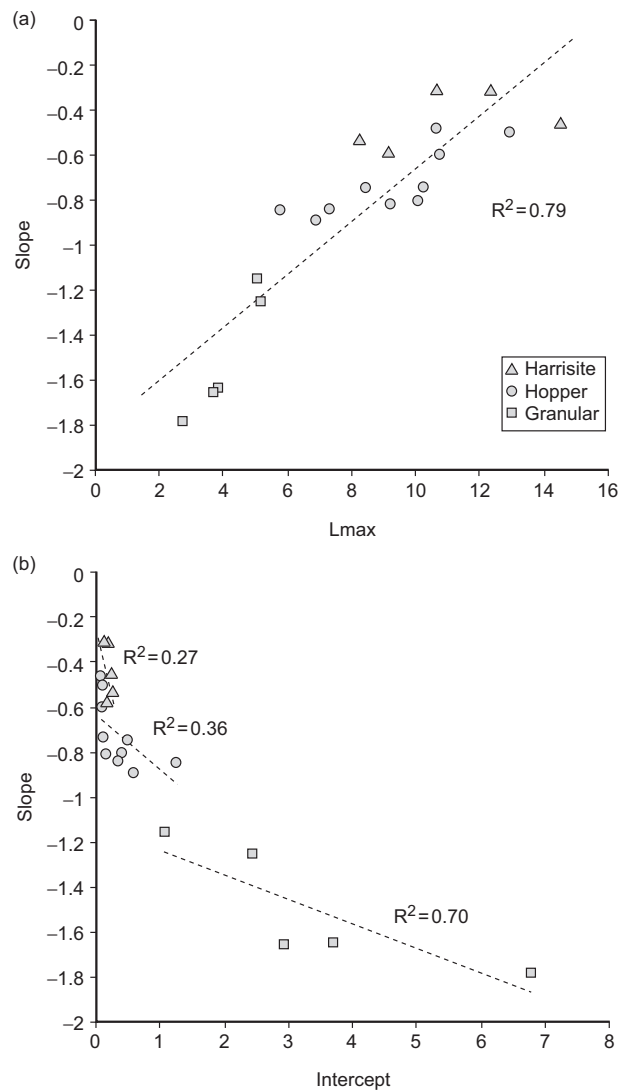


**Fig. 8.** (a) Regressed plots of slope vs  $L_{\max}$  and (b) slope vs intercept for the Rum CSD data. ( $R^2$  values calculated in Microsoft Excel.)

Rum harrisites and the feldspathic peridotites containing granular olivine morphologies. As suggested above, the granular olivine crystals are unlikely to have growth rates as high as predicted by Henderson & Williams (1979). Therefore, the slowest likely growth rate ( $10^{-7} \text{ mm/s}$ ) for harrisitic olivine together with the slowest growth rate for granular olivine ( $10^{-9} \text{ mm/s}$ ) are used to give minimum nucleation rates ( $\bar{J}_2$  and  $\bar{J}_3$ ; Table 3). These values of  $\bar{J}$  are in the range of  $(1.1\text{--}6.7) \times 10^{-9} \text{ mm}^{-3}/\text{s}$  for olivine in the feldspathic peridotite and  $(9.9\text{--}130) \times 10^{-9} \text{ mm}^{-3}/\text{s}$  for hopper and harrisitic olivine. Notably, values of  $\bar{J}$  for harrisite are now higher than those for granular textured peridotite, despite the fact that values of  $n^\circ$  remain the same.



**Fig. 9.** (a) Rhythmically layered feldspathic peridotite at Ard Mheall. (b) Linear train of fragmented olivine crystals in feldspathic peridotite. (c) Imbrication (highlighted) of fragmented harrisitic olivine crystals in feldspathic peridotite.

## REWORKED HARRISITIC OLIVINE IN GRANULAR-TEXTURED PERIDOTITE

Harrisite layers at Ard Mheall in the Western Layered Series are frequently interlayered with rhythmically layered feldspathic peridotite (Figs 2c and 9a) that exhibit evidence for deposition as cumulate 'sediments'. This includes sedimentary structures such as scour structures and slumping at layer interfaces. In addition, there is evidence in this area for periodic disruption of harrisite growth by small-scale, crystal-rich 'density' currents. Large fragmented harrisitic olivines have been incorporated into peridotitic cumulate overlying the harrisite layers, in which they exhibit structures that indicate they were reworked as single crystal clasts and as crystal clusters in flowing currents. These structures include linear trains (Fig. 9b) and imbricated fragments of broken olivines (Fig. 9c), and well-developed crystal lineations on layer planes. Based on their larger size than the equant (cumulus) olivine crystals native to the peridotite, these crystals are interpreted as fragments of harrisitic olivine. Their repeated occurrence throughout the sequence at Ard Mheall points to intervals of vigorous magmatic flow across the tops of harrisite layers, breaking the tops off crystals and terminating or suffocating harrisite development.

## DISCUSSION

### Harrisite petrogenesis

Wager *et al.* (1960) regarded harrisite as a type of cumulate texture in which skeletal and dendritic olivine grew upwards from previously 'deposited' cumulus crystals (crescumulate). Precipitation of olivine from a supercooled basaltic melt occurred onto those cumulus grains with upward-oriented *c*-axes; these olivines grew into a nuclei-deficient melt under tranquil conditions, following temporary cessation of convection of the magma. Donaldson (1974, 1977) pointed out that although this model explains the preferred upward olivine growth in most harrisite layers, it does not account for those olivines in some harrisite layers that are inferred to have grown downwards, horizontally, or in stellate arrangement. He also showed that some harrisite layers are in fact intrusive into the layers above and below them (Donaldson, 1982). In addition, Greenwood *et al.* (1990) and Upton *et al.* (2002) have presented evidence that picrite melts with 25–30 wt % olivine, rather than the basaltic melts envisaged by Wager *et al.* (1960), was involved on Rum.

Experimental studies suggest that skeletal hopper and branching crystals grow relatively rapidly under conditions of strong supersaturation or magmatic undercooling (e.g. Lofgren & Donaldson, 1975; Donaldson, 1976; Lofgren, 1980). Donaldson (1974, 1977) attributed harrisite

development to *in situ* crystallization under conditions of enhanced supersaturation of the magma in olivine. This he speculated might arise from two possible, alternative mechanisms; one is a sudden decrease in the water content of a water-undersaturated feldspathic peridotitic liquid, and the other the transition of a water-saturated peridotitic magma to an unsaturated state by exsolution of volatiles. Hort (1998) referred to harrisite as a disequilibrium texture developed through successive bursts of rapid crystallization as a result of periodic 'perturbations' of the liquidus temperature. He too suggested that exsolution of volatiles from magma could induce such an increase in undercooling, giving rise to the dendritic and skeletal crystal morphologies observed in harrisite texture. This he suggested could occur as a result of depressurization of a batch of magma during its ascent through the crust and would be most effective in shallow-level intrusions. Hort (1998) also pointed out that degassing of magma can occur where a more primitive melt enters a chamber and cools as a result of magma mixing with a more evolved melt.

### CSD data

The Rum CSD data are generally consistent throughout the localities studied. The CSD plots fall into three groups based on slope and intercept data calculated from regression analysis of each. This is well illustrated in Fig. 7b, which gives three groups of crystal morphology based on characteristic grain length vs volume phase proportion. The plot reflects decreasing crystal growth times and nucleation densities with increasing crystal morphological complexity. The majority of the granular peridotite CSD plots in Fig. 6 (e.g. R1, P1, R31B, R37) display pronounced convex-upward shapes at small size fractions as well as log-linear shapes at larger size fractions. Boorman *et al.* (2004) discussed the danger that cumulus textures may be strongly modified by crystal-ageing and compaction-driven recrystallization. It is thought that a downturn at small crystal sizes may indicate the consumption of smaller crystals at the expense of larger ones to minimize free energy as the primary cumulus textural arrangement equilibrated following deposition or *in situ* crystallization (Hunter, 1987; Waters & Boudreau, 1996; Higgins, 1998, 2002a; Park & Hanson, 1999). In addition to creating this 'humped' profile at small crystal sizes, this type of coarsening or ripening of primary igneous textures results in rotation of CSD plots to progressively shallower slopes (Marsh, 1998; Higgins, 2002a, 2006). For this reason, we feel that the crystal growth times calculated from the granular peridotite CSDs in this study may be useful only insofar as they might indicate possible greatest values of  $\tau$ .

In contrast, harrisitic olivines are a disequilibrium texture in which the olivines have large or very large surface areas and hence surface energy, yet in many cases

appear to have escaped subsequent textural equilibration or other postcumulus processes. For example, it is unlikely that compaction had a significant role to play in the development of the textures observed in harrisite, as thin-section petrography reveals a large (~50%) melt fraction in all of the samples (even those bearing an alignment of olivine crystals), represented by interstitial (intercumulus) unzoned plagioclase or clinopyroxene, which was apparently not expelled into the overlying magma. In addition, it might be expected that layers comprising vertically oriented harrisitic olivines would form a scaffold-like crystal arrangement that would be strongly resistant to compaction. Neither is there evidence of compaction-related processes such as compaction fractures or draping of olivine crystals around plagioclase or clinopyroxene oikocrysts as reported from other parts of the intrusion (Emeleus *et al.*, 1996). Another argument against significant recrystallization of harrisite is the cyclic nature of the sequences of magmatic layers they are confined within. The sequential change in olivine shape reported by Donaldson (1977; Figs 2c and 3) from simple granular forms to more complex crystal morphologies is observed in all areas where harrisite occurs. In these, particular types of olivine crystal morphology are often confined to certain layers; that is, there is a clear relationship between primary magmatic layering and crystal morphology, whereas significant recrystallization might have disrupted this relationship by causing complex crystal morphologies to grow towards simpler forms. We conclude that harrisite represents a primary magmatic, disequilibrium texture, essentially unmodified by recrystallization or textural equilibration, and the values of  $\tau$  calculated for harrisitic olivine are taken as reliable estimates for crystal growth times in this instance.

The extraordinarily short crystal growth times estimated from the CSDs are a function of the input growth rates used. There is experimental evidence to suggest that these rates are realistic (Lofgren & Donaldson, 1975; Lofgren, 1980). If the range of estimated crystal growth times presented is an accurate reflection of harrisite growth rates, then of particular interest is the rate at which individual harrisite layers crystallized. If an average crystal growth time of 8 h is taken for hopper olivines 10–20 mm in size (e.g.  $\tau_1$  in Table 3), then an average-sized layer, 500 mm thick, would crystallize in 8–17 days. Similar rates of crystallization (~15 days) are achieved by branching olivine layers of the same size. It is difficult to calculate a rate of thickening of layers containing granular olivines in the Rum cumulate pile, as it is very unlikely that granular olivines grew wholly *in situ*; that is, evidence described above suggests that peridotite layers accumulated by current deposition and magmatic flow processes.

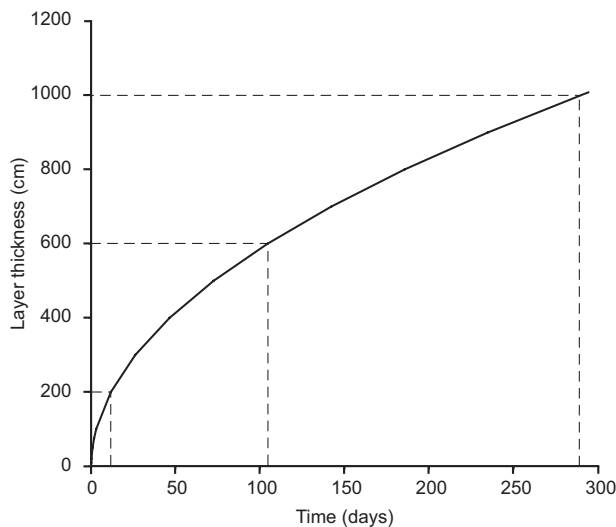


**Fig. 10.** Plot of cooling estimates of the time taken for harrisite layers to crystallize based on a range of values of layer thickness between a minimum of 7 cm and a maximum of 10 m (Donaldson, 1975a).

However, assuming rates of crystal accumulation similar to those for thickening of layers in the Skaergaard intrusion (0.6 mm/day; Wager & Brown, 1968) harrisite layers may have formed up to 160 times faster than normal cumulate layers.

Another indication of how rapidly harrisite layers formed can be obtained from a simple conductive cooling estimate of the time ( $t$ ) taken to cool a sheet of crystal mush or melt of half-thickness ( $L$ ), given by the equation

$$t \approx L^2/K$$

where  $K$  is the thermal diffusivity, which is  $1 \times 10^{-2} \text{ cm}^2/\text{s}$  (Jaeger, 1968). Given that harrisite layers range in thickness from 7 cm to 10 m (Donaldson, 1975a), a range of cooling times for harrisite layers are calculated and presented in Fig. 10. (The effect of taking latent heat of crystallization into account is to reduce each calculated layer thickness for a given time in Fig. 10 by  $\sim 30\%$ .) The calculations are consistent with the crystal growth times estimated from the CSDs, and suggest that the thinnest layers cooled fastest (e.g.  $\sim 11$  h for a 40 cm thick layer of harrisite). However, thicker layers are also shown to have cooled relatively rapidly, with values of 72 days and 290 days for 5 m and 10 m thick layers, respectively.

### Open-system behaviour of the Rum magma chamber during harrisite growth

A substantial body of evidence exists to suggest that open-system processes were a major influence in the history of the Rum magmatic system (Brown, 1956; Tait, 1985;

Emeleus *et al.*, 1996; Troll *et al.*, 2004). Much recent study on the ultrabasic and basic rocks of Rum has focused on the Eastern Layered Series, built of 16 macro-rhythmic peridotite–troctolite units (e.g. Tepley & Davidson, 2003; Holness, 2005). Although some debate persists as to the mode of construction of these units, it is generally accepted that most if not all of them represent major magma replenishment events (Emeleus *et al.*, 1996; Holness, 2005). Magmatic layering of minerals on the scale of millimetres to tens of centimetres is commonly observed within units of the Eastern Layered Series. In particular, the upper troctolitic section of each unit is associated with small-scale phase and rhythmic layering, resulting from numerous millimetre to centimetre-thick peridotite bodies interleaved with the troctolite. These thin peridotite bodies are mineralogically and texturally very similar in appearance to the much thicker peridotites that make up the lower portion of each unit, and suggest that replenishment may have involved both continual small influxes of magma, as well as intermittent large influxes of magma launching a new unit (Butcher *et al.*, 1985; Faithfull, 1985; Renner & Palacz, 1987). It is generally accepted that the Western Layered Series represents a deeper structural level of the Rum magma chamber, despite relations between the two being obscured by the younger Central Series. The Western Layered Series is also considered to have grown through periodic large volume influxes as well as smaller more frequent ones. Emeleus *et al.* (1996) pointed to the major north–south-trending Long Loch Fault, active throughout growth of the Rum Layered Suite, as the conduit for these magma influxes.

We argue that the approximately log–linear profiles and range of short crystal growth times given by the harrisitic olivine CSDs, combined with the nature of olivine growth in repeated sequences of magmatic layers, are additional strong evidence for open-system behaviour in the Western Layered Series. This leads to a petrogenetic model for harrisite layers in which the information supplied by the textural data on nucleation and growth of olivine in harrisite is applied to periodic small influxes of hot picrite magma over the floor of the Rum reservoir (Fig. 11).

Prior to harrisite formation a major batch of magma nucleated and grew olivine at the base of the intrusion, with magmatic sedimentation and crystal accumulation through small-scale density current action giving rise to magmatic layering of feldspathic peridotite with associated sedimentary structures (Fig. 11a). The chamber was then replenished by a small batch of hotter, denser picrite magma that spread thinly along the bottom of the chamber and cooled against the colder magma above (Fig. 11b). It is assumed that the inflowing magma contained very sparse or no olivine crystals, so that for

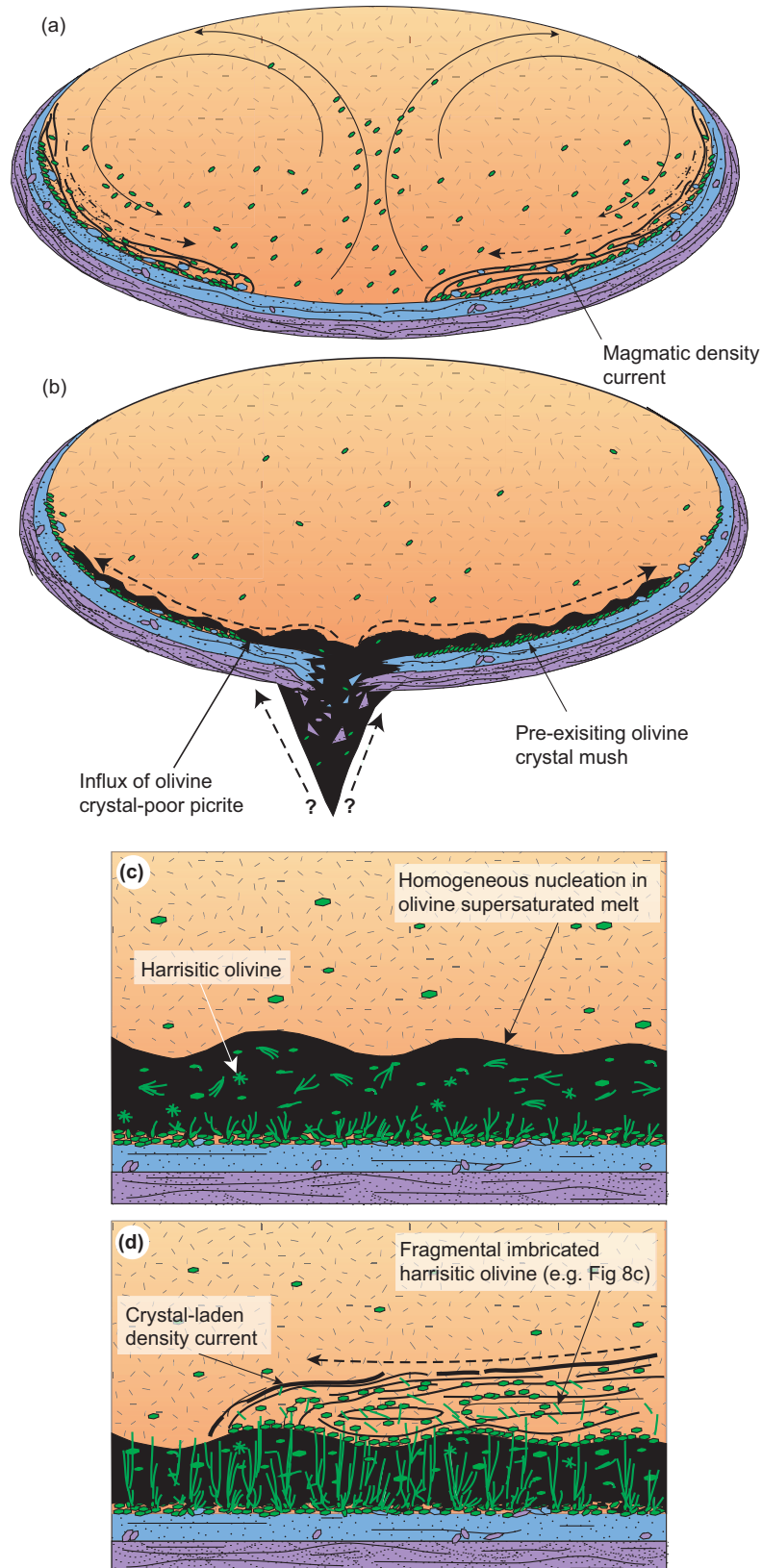


**Fig. 11.** (a)–(d) Schematic diagrams of the Rum magma chamber throughout the development of a harrisitic layer (see text for description).

solidification to commence homogeneous, rather than heterogeneous, nucleation of olivine was necessary (Fig. 11b). Thus there was a delay in nucleation during which the melt undercooled (Donaldson, 1979), creating the necessary enhanced olivine supersaturation for homogeneous olivine nucleation as well as promoting skeletal growth (Fig. 11c). Upon nucleation, fast bursts of *in situ* skeletal olivine growth occurred throughout the batch of picrite magma, occasionally producing stellate or 'starburst' crystals. It is also envisaged that sometimes rapid precipitation of olivine occurred from the picrite melt onto the crystal mush below, triggering harrisite growth from the substrate, where cumulus crystals with their *c*-axes oriented subvertically outgrew their neighbours (Fig. 11c; see Wadsworth, 1961). A recent experimental study of olivine growth suggests that such constrained growth may require the presence of a significant vertical temperature gradient (Faure *et al.*, 2006).

It is considered that sheets of picrite magma containing significant amounts of crystals and nuclei might not have developed harrisitic texture, as the crystals would have provided sites for heterogeneous nucleation and thus precluded intense supersaturation of olivine.

Cessation of harrisite development may have resulted from the complete crystallization of a thin batch of picrite magma as outlined above. Alternatively, the passage of crystal-laden density currents over the top of the growing layer of harrisite crystals, as inferred from evidence at Ard Mheall (Figs 9b, c and 11d) may have occasionally terminated harrisite formation. Convective overturn when the density of the picrite magma approached that of the overlying magma and attendant crystals could also have terminated skeletal crystal growth.

We propose that repeated periodic influxes of crystal-poor picrite produced the sequence of harrisite layers of variable thickness observed at Harris Bay and Ard Mheall in the Western Layered Series. The presence of minor harrisite layers high up in the Eastern Layered Series (i.e. Units 13–15) suggests that crystal-poor picrite magma was still available at this later stage in the development of the Rum Layered Suite, although possibly in much smaller quantities (see also Upton *et al.*, 2002).

Recognition that the open-system behaviour of magma emplacement in the Rum magma chamber included small-volume crystal-poor magma inputs, which experienced an enhanced cooling rate as they spread across the floor, removes the need to invoke supersaturation effects arising from decompression of large influxes of H<sub>2</sub>O-saturated magma or repeated exsolution of H<sub>2</sub>O once the magma entered the chamber (Donaldson, 1974; Hort, 1998). Absence of rocks in the Rum Layered Suite that show the effects of explosions and retention of the delicate dendritic olivines in many harrisite layers are consistent with this inference.

## CONCLUSIONS

In this study we have employed detailed textural quantification using CSD analysis and incorporating published olivine growth rates and experimental data to evaluate the formation of harrisite and granular olivine textures in the Rum intrusion, NW Scotland, with the following conclusions.

- (1) Influxing batches of crystal-poor picrite magma at the base of the Rum magma chamber undercooled upon contact with the cooler magma already in place.
- (2) The delay in homogeneous nucleation of olivine and consequent elevated supersaturation of the picrite in an olivine component gave rise to the harrisitic texture.
- (3) Periods of rapid crystal growth lasted on the order of hours to days. Using the textural data available at present, our estimates range from several hours to several hundreds of days.
- (4) The repeated occurrence of harrisite throughout the Western Layered Series, and to a lesser degree the Eastern Layered Series, is consistent with the concept of 'leaky' open-system behaviour of the Rum magma chamber.

## ACKNOWLEDGEMENTS

Liz McCourt and Kris O'Dowd are thanked for their help at various stages of this work. We also acknowledge the technical assistance of Neil Kearney and Declan Burke. Scottish Natural Heritage granted permission to conduct fieldwork on the Isle of Rum. John Gamble provided constructive comments on an earlier version of the manuscript, and the insightful and positive reviews of Michael Higgins, Gary Lofgren and Bruce Marsh are gratefully acknowledged. B.O'D. acknowledges receipt of an Irish Research Council for Science Engineering and Technology (IRCSET) grant for postgraduate study at Trinity College Dublin, and support from a Mineralogical Society Bursary. V.R.T. acknowledges support from Science Foundation Ireland.

## REFERENCES

- Boorman, S., Boudreau, A. & Kruger, F. J. (2004). The Lower Zone–Critical Zone transition of the Bushveld Complex: a quantitative textural study. *Journal of Petrology* **45**, 1209–1235.
- Brown, G. M. (1956). The layered ultrabasic rocks of Rhum, Inner Hebrides. *Philosophical Transactions of the Royal Society of London, Series B* **240**, 1–53.
- Burton, J. A., Prim, R. C. & Slichter, W. P. (1953). The distribution of solute from crystals grown from the melt. Part I: Theoretical. *Journal of Chemical Physics* **21**, 1987–1999.
- Butcher, A. R., Young, I. M. & Faithfull, J. W. (1985). Finger structures in the Rhum Complex. *Geological Magazine* **122**, 503–518.

- Cashman, K. V. (1993). Relationship between plagioclase crystallization and cooling rate in basaltic melts. *Contributions to Mineralogy and Petrology* **113**, 126–142.
- Cashman, K. V. & Marsh, B. D. (1988). Crystal size distribution (CSD) in rocks and the kinetics and dynamics of crystallisation II: Makaopuhi lava lake. *Contributions to Mineralogy and Petrology* **99**, 292–305.
- Coogan, L. A., Thompson, G. & MacLeod, C. J. (2002). A textural and geochemical investigation of high level gabbros from the Oman ophiolite: implications for the role of the axial magma chamber at fast spreading ridges. *Lithos* **63**, 67–82.
- Donaldson, C. H. (1974). Olivine crystal types in harrisitic rocks of the Rhum pluton and in Archean spinifex rocks. *Geological Society of America Bulletin* **85**, 1721–1726.
- Donaldson, C. H. (1975a). A petrogenetic study of harrisite in the Isle of Rhum pluton, Scotland. Ph.D. thesis, University of St Andrews, 138 pp.
- Donaldson, C. H. (1975b). Calculated diffusion coefficients and the growth rate of olivine in a basalt magma. *Lithos* **8**, 163–174.
- Donaldson, C. H. (1976). An experimental investigation of olivine morphology. *Contributions to Mineralogy and Petrology* **57**, 187–213.
- Donaldson, C. H. (1977). Laboratory duplication of comb layering in the Rhum pluton. *Mineralogical Magazine* **41**, 323–336.
- Donaldson, C. H. (1979). An experimental investigation of the delay in nucleation of olivine in mafic magmas. *Contributions to Mineralogy and Petrology* **69**, 21–32.
- Donaldson, C. H. (1982). Origin of some of the Rhum harrisite by segregation of intercumulus liquid. *Mineralogical Magazine* **45**, 201–209.
- Emeleus, C. H., Cheadle, M. J., Hunter, R. H., Upton, B. G. J. & Wadsworth, W. J. (1996). The Rum Layered Suite. In: Cawthorn, R. G. (ed.) *Layered Igneous Rocks*. Amsterdam: Elsevier, pp. 403–440.
- Faithfull, J. W. (1985). The Lower Eastern Layered Series of Rhum. *Geological Magazine* **122**, 459–468.
- Faure, F., Troliard, G., Nicollet, C. & Montel, J. M. (2003). A developmental model of olivine morphology as a function of the cooling rate and the degree of undercooling. *Contributions to Mineralogy and Petrology* **145**, 251–263.
- Faure, F., Arndt, N. & Libourel, G. (2006). Formation of spinifex texture in komatiites: an experimental study. *Journal of Petrology* **47**, 1591–1610.
- Greenwood, R. C., Donaldson, C. H. & Emeleus, C. H. (1990). The contact zone of the Rhum ultrabasic intrusion: evidence of peridotite formation from magnesian magmas. *Journal of the Geological Society, London* **147**, 209–212.
- Gualda, A. R. (2006). Crystal size distributions derived from 3D datasets: sample size versus uncertainties. *Journal of Petrology* **47**, 1245–1254.
- Harker, A. (1908). *The Geology of the Small Isles of Inverness-shire*. Memoir of the Geological Survey of Scotland.
- Henderson, P. & Williams, C. T. (1979). Variation in trace element partition (crystal/magma) as a function of crystal growth rate. In: Ahrens, L. H. (ed.) *Origin and Distribution of the Elements*. Oxford: Pergamon, pp. 191–198.
- Henderson, P., MacKinnon, A. & Gale, N. H. (1971). The distribution of uranium in some basic igneous cumulates and its petrological significance. *Geochimica et Cosmochimica Acta* **35**, 917–925.
- Higgins, M. D. (1994). Numerical modelling of crystal shapes in thin-sections; estimation of crystal habit and true size. *American Mineralogist* **79**, 113–119.
- Higgins, M. D. (1996). Crystal size distribution and other quantitative textural measurements in lavas and tuffs from Egmon volcano (Mt. Taranaki), New Zealand. *Bulletin of Volcanology* **58**, 194–204.
- Higgins, M. D. (1998). Origin of anorthosite by textural coarsening: quantitative measurements of a natural sequence of textural development. *Journal of Petrology* **39**, 1307–1323.
- Higgins, M. D. (2000). Measurement of crystal size distributions. *American Mineralogist* **85**, 1105–1116.
- Higgins, M. D. (2002a). The role of textural coarsening in the development of the Kiglapait layered mafic intrusion, Labrador, Canada: a crystal size distribution study. *Contributions to Mineralogy and Petrology* **144**, 314–330.
- Higgins, M. D. (2002b). Closure in crystal size distributions (CSD), verification of CSD calculations, and the significance of CSD fans. *American Mineralogist* **87**, 171–175.
- Higgins, M. D. (2006). Use of appropriate diagrams to determine if crystal size distributions (CSD) are dominantly semi-logarithmic, lognormal or fractal (scale invariant). *Journal of Volcanology and Geothermal Research* **154**, 8–16.
- Hofmann, A. W. (1980). Diffusion in nature; silicate melts: a critical review. In: Hargraves, R. B. (ed.) *Physics of Magmatic Processes*. Princeton, NJ: Princeton University Press, pp. 385–417.
- Holness, M. B. (2005). Spatial constraints on magma chamber replenishment events from textural observations of cumulates: the Rum Layered Intrusion, Scotland. *Journal of Petrology* **46**, 1585–1600.
- Hort, M. (1998). Abrupt change in magma liquidus temperature because of volatile loss or magma mixing: effects on nucleation, crystal growth and thermal history of the magma. *Journal of Petrology* **39**, 1064–1076.
- Hunter, R. H. (1987). Textural equilibrium in layered igneous rocks. In: Parsons, I. (ed.) *Origins of Igneous Layering*. Dordrecht: Reidel, pp. 473–503.
- Jaeger, J. C. (1968). Cooling and solidification of igneous rocks. In: Hess, H. H. & Poldervaart, A. (eds) *Basalts, The Poldervaart Treatise on Rocks of Basaltic Composition*. New York: John Wiley, pp. 503–537.
- Jambon, A., Lussiez, P., Clochiatti, R., Weisz, J. & Hernandez, J. (1992). Olivine growth rates in a tholeiitic basalt: an experimental study of melt inclusions in plagioclase. *Chemical Geology* **96**, 277–287.
- Jerram, D. A. (2001). Visual comparators for degree of sorting in 2-D and 3-D. *Computers and Geoscience* **27**, 485–492.
- Jerram, D. A. & Cheadle, M. J. (2000). On the cluster analysis of rocks. *American Mineralogist* **84**(1), 47–67.
- Jerram, D. A. & Kent, A. J. R. (2006). An overview of modern trends in petrography: textural and microanalysis of igneous rocks. *Journal of Volcanology and Geothermal Research* **154**, 7–9.
- Jerram, D. A., Cheadle, M. J., Hunter, R. H. & Elliott, M. T. (1996). The spatial distribution of grains and crystals in rocks. *Contributions to Mineralogy and Petrology* **125**(1), 60–74.
- Jerram, D. A., Cheadle, M. J. & Philpotts, A. R. (2003). Quantifying the building blocks of igneous rocks: are clustered crystal frameworks the foundation?. *Journal of Petrology* **44**, 2033–2051.
- Kohut, E. J. & Nielsen, R. L. (2004). Melt inclusion formation mechanisms and compositional effects in high-An feldspar and high-Fo olivine in anhydrous mafic silicate liquids. *Contributions to Mineralogy and Petrology* **147**, 684–704.
- Lofgren, G. E. (1980). Experimental studies on the dynamic crystallization of silicate melts. In: Hargraves, R. B. (ed.) *Physics of Magmatic Processes*. Princeton, NJ: Princeton University Press, pp. 487–551.
- Lofgren, G. E. & Donaldson, C. H. (1975). Curved branching crystals and differentiation in comb-layered rocks. *Contributions to Mineralogy and Petrology* **49**, 309–319.

- Marsh, B. D. (1988). Crystal size distribution (CSD) in rocks and the kinetics and dynamics of crystallisation I: Theory. *Contributions to Mineralogy and Petrology* **99**, 277–291.
- Marsh, B. D. (1996). Solidification fronts and magmatic evolution. *Mineralogical Magazine* **60**, 5–40.
- Marsh, B. D. (1998). On the interpretation of crystal size distributions in magmatic systems. *Journal of Petrology* **39**, 553–599.
- Mock, A. & Jerram, D. A. (2005). Crystal size distributions (CSD) in three dimensions: insights from the 3D reconstruction of a highly porphyritic rhyolite. *Journal of Petrology* **46**(8), 1525–1541.
- Morgan, D. J. & Jerram, D. A. (2006). On estimating crystal shape for crystal size distribution analysis. *Journal of Volcanology and Geothermal Research* **154**, 1–7.
- Park, Y. & Hanson, B. (1999). Experimental investigation of Ostwald-ripening rates of forsterite in the haplobasaltic system. *Journal of Volcanology and Geothermal Research* **90**, 103–113.
- Renner, R. & Palacz, Z. A. (1987). Basaltic replenishment of the Rhum magma chamber: evidence from unit 14. *Journal of the Geological Society, London* **144**, 961–970.
- Resmini, R. G. & Marsh, B. D. (1995). Steady-state volcanism, paleoeffusion rates, and magma system volume inferred from plagioclase crystal size distributions in mafic lavas; Dome Mountain, Nevada. *Journal of Volcanology and Geothermal Research* **68**(4), 273–296.
- Roggensack, K. (2001). Sizing up crystals and their melt inclusions: a new approach to crystallisation studies. *Earth and Planetary Science Letters* **187**, 221–237.
- Seitz, M. G. (1974). Promotion of kinetic disequilibrium of trace thorium. *Carnegie Institution of Washington Yearbook* **73**, 551–553.
- Tait, S. R. (1985). Fluid dynamic and geochemical evolution of cyclic unit 10, Rhum, Eastern Layered Series. *Geological Magazine* **122**, 555–568.
- Taubeneck, W. H. & Poldervaart, A. (1960). Geology of the Elkhorn mountains, Northeastern Oregon: Part 2. Willow Lake intrusion. *Geological Society of America Bulletin* **71**, 1295–1322.
- Tepley, F. J. & Davidson, J. P. (2003). Mineral-scale Sr-isotope constraints on magma evolution and chamber dynamics in the Rum layered intrusion, Scotland. *Contributions to Mineralogy and Petrology* **145**, 628–641.
- Troll, V. R., Donaldson, C. H. & Emeleus, C. H. (2004). Pre-eruptive magma mixing in intra-caldera ash-flow deposits of the Rum Igneous Centre, Scotland. *Contributions to Mineralogy and Petrology* **147**, 722–739.
- Turner, S., George, R., Jerram, D. A., Hawkesworth, C. & Carpenter, N. (2003). Case studies of plagioclase growth and residence times in island arc lavas from Tonga and the Lesser Antilles and a model to reconcile discordant age information. *Earth and Planetary Science Letters* **214**, 279–294.
- Upton, B. G. J., Skovgaard, A. C., McClurg, J., Kirstein, L., Cheadle, M., Emeleus, C. H., Wadsworth, W. J. & Fallick, A. E. (2002). Picritic magmas and the Rum ultramafic complex, Scotland. *Geological Magazine* **139**(4), 437–452.
- Wadsworth, W. J. (1961). The layered ultrabasic rocks of south-west Rhum, Inner Hebrides. *Philosophical Transactions of the Royal Society of London, Series B* **244**, 21–64.
- Wager, L. R. & Brown, G. M. (1968). *Layered Igneous Rocks*. Edinburgh: Oliver and Boyd, 588 pp.
- Wager, L. R., Brown, G. M. & Wadsworth, W. J. (1960). Types of igneous cumulates. *Journal of Petrology* **1**, 73–85.
- Waters, C. & Boudreau, A. E. (1996). A reevaluation of crystal size distributions in chromite cumulates. *American Mineralogist* **81**, 1452–1459.
- Zieg, M. J. & Lofgren, G. E. (2006). An experimental investigation of texture evolution during continuous cooling. *Journal of Volcanology and Geothermal Research* **154**, 74–88.